[9] K. K. Mei, "On the integral equations of thin wire antennas," *IEEE Trans. Antennas Propagat.*, vol. AP-13, pp. 374–378, May 1965.
[10] J. Perini and D. J. Buchanan, "Assessment of MOM techniques for shipboard applications," *IEEE Trans. Electromagn. Compat.*, vol. EMC-24, pp. 32–39, Feb. 1982.
[11] C. M. Butler and D. R. Wilton, "Analysis of various numerical techniques applied to thin-wire scatters," *IEEE Trans Antennas Propagat.*, vol. AP-23, pp. 534–540, July 1975.
[12] B. D. Popovic, "Polynomial approximation of current along thin symmetrical cylindrical dipoles," *Proc. IEE*, vol. 117, pp. 837–878, May 1970.
[13] I.E.C. Document 12A (Secretariat) 208, July 1980.
[14] L. C. Middlekamp, Private communication to Mr. M. Okamura.
[15] I.E.C. Document 12A (Central Office) 108, Oct. 1981.
[16] M. Borsero and E. Nano, "Comparison between calculated and measured attenuation of the site recommended by IEC for radiation measurements," presented at 4th Symp. Tech. Exhibition EMC (Zurich, Switzerland), 80N4, Mar. 1981.
[17] I.E.C. Document 12A (Tokyo/Japan) 1, Oct. 1980.

A Novel Method to Analyze Electromagnetic Scattering of Complex Objects

KORADA UMASHANKAR, SENIOR MEMBER, IEEE, AND ALLEN TAFLOVE, MEMBER, IEEE

Abstract—**The finite-difference time-domain (FD-TD) method is proposed as a means of accurately computing electromagnetic scattering by arbitrary-shaped extremely complex metal or dielectric objects excited by an external plane wave. In the proposed method, one first uses the FD-TD method to compute the near total fields within a rectangular volume which fully encloses the object. Then, an electromagnetic-field equivalence principle is invoked at a virtual surface of this rectangular volume to transform the tangential near scattered fields to the far field. To verify the feasibility of this method, the surface currents, near scattered fields, far scattered fields, and radar cross section of two canonical two-dimensional objects are presented. For these cases, it is shown that the FD-TD method provides magnitude of current and field predictions which are within ±2.5 percent and further phase values within ±3° of values predicted by the method of moments (MOM) at virtually every point including in shadow regions.**

Key Words—**Electromagnetic scattering, complex objects, finite-difference time-domain method, equivalence principle, surface current, near scattered fields, far fields, radar cross section.**

I. INTRODUCTION

GENERAL electromagnetic scattering problems have been difficult to treat with either analytical [1] or numerical methods because of the complicating effects of curvatures, corners, apertures, and dielectric loading of structures. In an attempt to gain insight into scattering mechanisms using analytical and numerical approaches, it has been necessary to use canonical structures rather than realistic models. A potential alternate approach is the finite-difference time-domain (FD-TD) method [2]-[17] which allows the computation of internal and external near fields by direct modeling of realistic structures.

In order to treat realistic scattering problems effectively, a method has been developed [14], [15], [17] which involves combining the FD-TD method with a near-field to far-field transformation using field equivalences [18]. In this method, the scattering problem is analyzed in two steps by treating the relatively complex near-field region and the relatively simple far-field region separately. The method involves first the determination of equivalent electric and/or magnetic currents tangential to a virtual surface surrounding the scatterer of interest by using the FD-TD method for a given external illumination. The computed near-field equivalent currents are then transformed to derive the far-field scattering pattern and the radar cross section. Since the FD-TD method can deal with dielectric, permeable, and inhomogeneous materials in a natural manner, it is possible to incorporate most of the physics of wave interaction with any complex scatterer of interest.

To validate feasibility of this hybrid method, the FD-TD computed surface electric-current distribution and near scattered electric and magnetic fields are presented for the case of a rectangular metal cylinder subject to plane-wave illumination at normal and oblique incidence. These currents and scattered fields are compared to method of moments (MOM) computed results. The far scattered field pattern and radar cross section

Manuscript received March 26, 1982; revised July 6, 1982. This work was supported in part by Rome Air Development Center, Griffiss Air Force Base, NY, under Air Force Contract F30602-80-C-0302, and in part by the Internal Research of the Electronics Division, ITT Research Institute, Chicago, IL 60616.

The authors are with the IIT Research Institute, Chicago, IL 60616. (312) 567-4489.

0018-9375/82/1100-0397$00.75

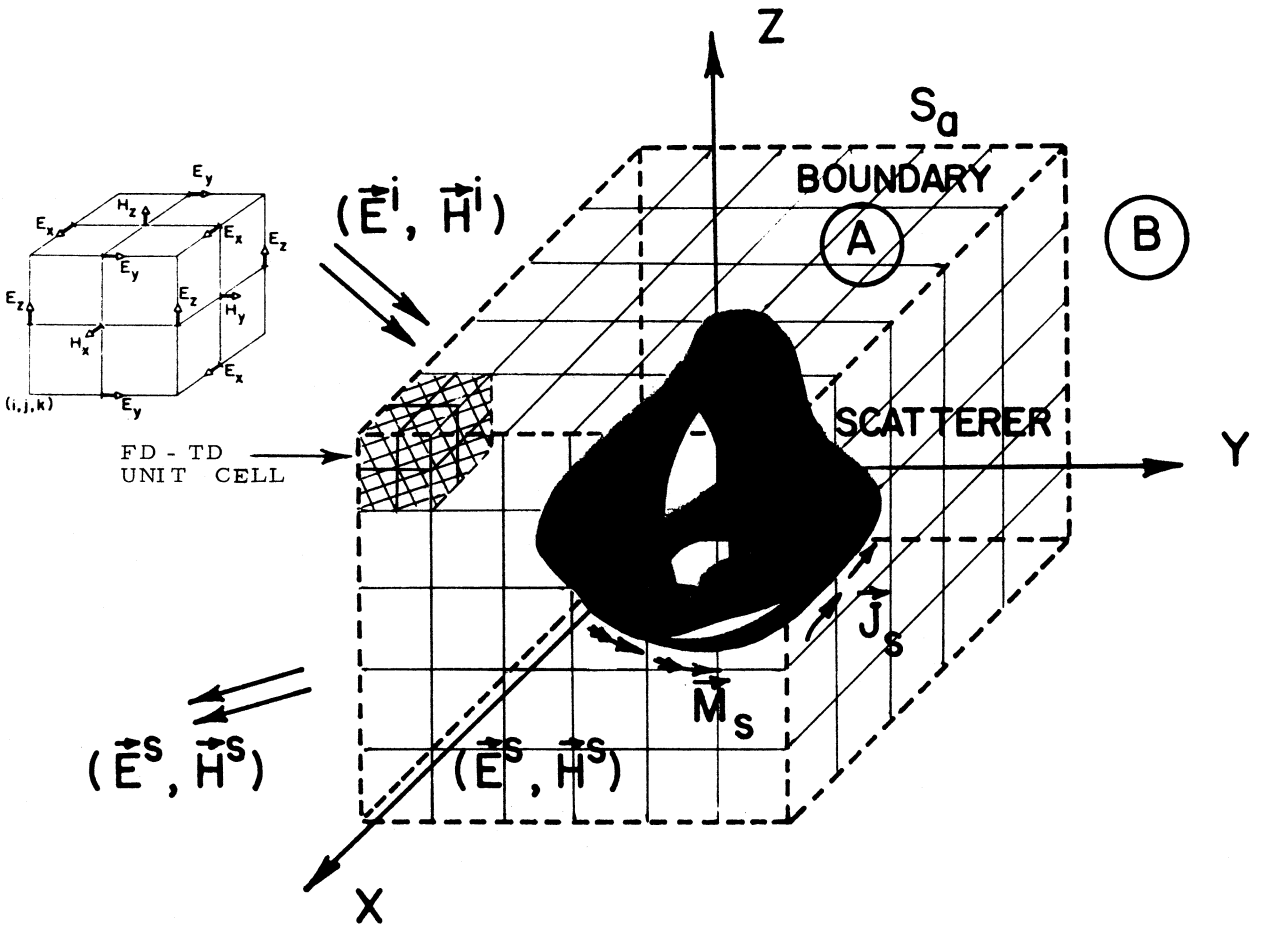

Fig. 1. Geometry of a general scatterer in free-space medium and FD-TD lattice arrangement.

are derived from the FD-TD data using a near- to far-field transformation and are also compared to the results obtained using MOM [19]. It is shown that a very high degree of correspondence is obtained using this proposed method.

II. FORMULATION

A brief enumeration of the steps to analyze scattering by complex objects is presented in this section, based on the application of the FD-TD method to obtain the near fields, and then the transformation of the near fields to far fields to obtain the scattering cross section. In Fig. 1 is shown a geometry of an arbitrary-shaped scattering object. This object can be either conducting, dielectric, or permeable as well as inhomogeneous. It can have apertures/cavities containing internal dielectric loading [9], [10]. The incident field $(\boldsymbol{E}^i, \boldsymbol{H}^i)$ excites the scatterer to produce, simultaneously, some interior-field penetration and also an exterior scattered field $(\boldsymbol{E}^s, \boldsymbol{H}^s)$.

A. Near-Field Analysis

As shown in Fig. 1, the scatterer is enclosed in a rectangular volume with a boundary surface S_a for analyzing the near total fields based on FD-TD [9], [10], [14], [15], [17]. The finite-difference formulation of the FD-TD method allows a straight-forward modeling of the surfaces and interiors of arbitrary complex structures. The structure of interest is mapped into the space lattice, Fig. 1, by first choosing the space increment [10] and assigning values of permittivity and conductivity to each component of total electric field $\boldsymbol{E}$. No special handling of electromagnetic boundary conditions at media interfaces is required because the curl equations generate these conditions in a natural way [10]. The various details of the structure are modeled with a maximum resolution of one unit cell, with thin surfaces being modeled as stepped-edge sheets. The explicit numerical formulation of the FD-TD method is particularly suited for programming with minimum storage and execution time using recently developed array-processing computers. The required computer storage and running time increases only linearly with N, where N is the total number of unknown field components [9]. Since all FD-TD operations are explicit and can be performed in parallel, rapid array-processing techniques can be readily applied. As demonstrated [9], [10], these can be used to solve for more than 10^6 field components in a single FD-TD problem (current array-processing capability).

As discussed in [9], [10], the FD-TD method is a direct numerical solution to the Maxwell's time-dependent curl equations useful for studying propagation of an electromagnetic wave into a volume of space containing an arbitrary-shaped dielectric or conducting body. By time-stepping or repeatedly implementing a finite-difference analog of the curl equations at each cell (Fig. 1) of the corresponding space lattice, the incident wave is tracked as it first propagates to the structure

and then interacts with it via penetration and diffraction. Wave tracking is completed when the desired late-time or sinusoidal steady-state behavior is observed at each lattice cell. The time-stepping for the FD-TD method is accomplished by positioning the components of E and H about a unit cell of the lattice, as shown in Fig. 1, and evaluating E and H at alternate half-time steps. Centered difference expressions can be used for both the space and time derivatives to attain second-order accuracy in the space and time increments.

The following discussion briefly summarizes important new features of the FD-TD method. A more complete discussion is contained in [15], [17].

1) FD-TD Lattice Regions and Plane-Wave Source Condition [12], [14]-[17]: As shown in Fig. 2(a), the latest formulation of the FD-TD lattice involves the division of the computation space into two distinct regions, separated by a rectangular surface which serves to connect fields in each region. In 2 dimensions, the surface has 4 faces; in 3 dimensions, the surface has 6 faces.

Region 1 of the FD-TD lattice is denoted as the *total-field* region. Here, it is assumed that all computed field quantities are comprised of the sum of the incident wave and the scattered field. The interacting structure of interest is embedded within this region.

External to Region 1 is Region 2 of the FD-TD lattice which is denoted as the *scattered-field* region. Here, it is assumed that all computed field quantities are comprised only of the scattered field. The outer lattice planes bounding Region 2, called the *lattice truncation planes*, serve to implement the free-space radiation condition.

The rectangle faces comprising the boundary between Regions 1 and 2 contain E and H field components which require the formulation of various field-component differences across the boundary planes for proceeding one time step. Typical FD-TD computations at these boundary points are as follows, using the spatial coordinates shown in Fig. 2(b):

$$\tilde{E}_z^{n+1}(i, j_0) = \tilde{E}_z^{n+1}(i, j_0)\Big|_{\substack{\text{ordinary FD-TD}\\ \text{analog [9]}}} + C_b(m) H_x^{i\,n+1/2}(i, j_0 - \tfrac{1}{2}) \tag{1a}$$

$$H_x^{n+1/2}(i, j_0 - \tfrac{1}{2}) = H_x^{n+1/2}(i, j_0 - \tfrac{1}{2})\Big|_{\substack{\text{ordinary FD-TD}\\ \text{analog [9]}}} + \tilde{E}_z^{\,in}(i, j_0). \tag{1b}$$

Here, $\tilde{E}_z^{n+1}(i, j_0)$ is the usual FD-TD value of the *total* E_z component evaluated at point (i, j_0) and time step $n + 1$. Similarly, $H_x^{n+1/2}(i, j_0 - \frac{1}{2})$ is the usual FD-TD value of the *scattered* H_x^s component evaluated at point $(i, j_0 - \frac{1}{2})$ and time step $n + \frac{1}{2}$. $C_b(m)$ denotes a proportionality factor defined in [9], [15], [17]. The superscript i denotes the incident field component value. These computations serve to *connect* the total-field and scattered-field regions *and* simultaneously generate the desired plane wave of arbitrary polarization and angle of incidence [14]-[17]. An alternative approach for incident-wave generation based on the Huygen's source formulation is discussed in [12].

There are a number of key advantages to this methodology.

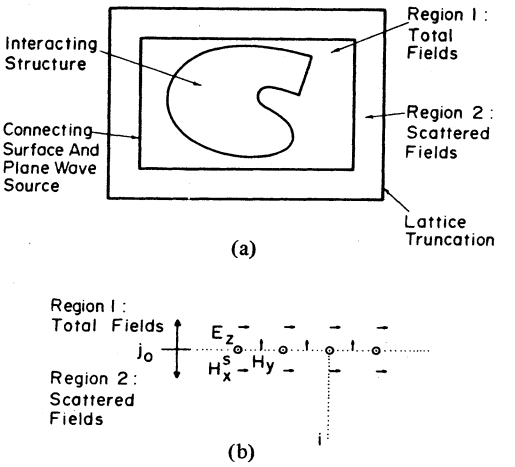

Fig. 2. Division of FD-TD lattice into total-field and scattered-field regions. (a) Lattice division. (b) Typical connecting conditions between regions.

a) The total-field formalism is retained for the entirety of the interacting structure, permitting accurate computations of low-level fields penetrating into cavities through apertures, and in the shadow regions of scatterers. b) The scattered-field formalism is retained for the lattice truncation region, permitting a very accurate simulation of the radiation condition. c) The incident wave contribution need be computed or stored only for the field components at the rectangular surface connecting Regions 1 and 2. This results in much less computation or storage than if the incident field were to be computed at all points within the interacting structure to implement a pure scattered-field formalism. d) The scattered near field in Region 2 can be easily integrated to derive the far-field scattering and radar cross section, as discussed later in this paper.

2) Lattice Truncation Conditions [3]-[5], [8], [15]-[17], [20], [21]: A basic consideration with the FD-TD approach to solve electromagnetic-field problems is that most such problems are usually considered to be "open" problems where the domain of the computed field is ideally unbounded. Clearly, no computer can store an unlimited amount of data, and the field computation zone must be limited. The computation zone must be large enough to enclose the structure of interest, and a suitable boundary condition on the outer perimeter of the computation zone must be used to simulate the extension of the computation zone to infinity. Outer boundary conditions of this type have been called either radiation conditions, absorbing boundary conditions, or lattice truncation conditions.

In 3 dimensions, an outgoing scattered-wave field component F^s (either an electric or magnetic field) has a (r, θ, ϕ) variation of the type [22]

$$F^s = F_0 e^{j(\omega t - k_0 r)}\left[\frac{A(\theta, \phi)}{r} + \frac{B(\theta, \phi)}{r^2} + \cdots\right]. \tag{2}$$

Here, the bracketed infinite series represents, in effect, a multipole expansion of the scattered field, where A, B, ..., are initially unknown functions of angular position.

First-order FD-TD simulations of the outer lattice bound-

ary condition approximate the $A(\theta, \phi)/r$ dependence only. Second- and higher order approximations simulate the $B(\theta,\phi)/r^2$ and higher order r-dependent behavior of F^s in addition to the $A(\theta, \phi)/r$ term [15]. A typical FD-TD computation realizing a second-order correct radiation condition [16] is given by

$$\begin{aligned}\tilde{E}_z^{n+1}(0,j,k+\tfrac{1}{2}) &= -\tilde{E}_z^{n-1}(1,j,k+\tfrac{1}{2}) + \frac{c\delta t-\delta}{c\delta t+\delta} \cdot [\tilde{E}_z^{n+1}(1,j,k+\tfrac{1}{2}) + \tilde{E}_z^{n-1}(0,j,k+\tfrac{1}{2})] \\ &+ \frac{2\delta}{c\delta t+\delta}[\tilde{E}_z^{n}(0,j,k+\tfrac{1}{2}) + \tilde{E}_z^{n}(1,j,k+\tfrac{1}{2})] \\ &+ \frac{(c\delta t)^2}{2\delta(c\delta t+\delta)} \cdot \begin{bmatrix} \tilde{E}_z^{n}(0,j+1,k+\tfrac{1}{2}) - 2\tilde{E}_z^{n}(0,j,k+\tfrac{1}{2}) \\ \quad + \tilde{E}_z^{n}(0,j-1,k+\tfrac{1}{2}) \\ +\tilde{E}_z^{n}(1,j+1,k+\tfrac{1}{2}) - 2\tilde{E}_z^{n}(1,j,k+\tfrac{1}{2}) \\ \quad + \tilde{E}_z^{n}(1,j-1,k+\tfrac{1}{2}) \\ +\tilde{E}_z^{n}(0,j,k+\tfrac{3}{2}) - 2\tilde{E}_z^{n}(0,j,k+\tfrac{1}{2}) \\ \quad + \tilde{E}_z^{n}(0,j,k-\tfrac{1}{2}) \\ +\tilde{E}_z^{n}(1,j,k+\tfrac{3}{2}) - 2\tilde{E}_z^{n}(1,j,k+\tfrac{1}{2}) \\ \quad + \tilde{E}_z^{n}(1,j,k-\tfrac{1}{2}) \end{bmatrix}. \end{aligned} \tag{3}$$

In (3), $\tilde{E}_z^{n+1}(0, j, k + \frac{1}{2})$ is the desired truncation-plane value of $\tilde{E}_z$ at point $(0, j, k + \frac{1}{2})$; δ is the lattice cell size; and δt is the time step. Analogous conditions can be written for the five other truncation planes (in three-dimensional problems). The accuracy of this formulation is discussed in [16], [20].

3) Sinusoidal Steady-State Information: Such data can be obtained either by a) directly programming a single-frequency incident plane wave or b) performing a separate Fourier transformation step on the pulse waveform response. Both methods require time-stepping to a maximum time equal to several wave periods at the desired frequency. The second method has two additional requirements. First, a short-rise-time pulse suffers from accumulating waveform error due to overshoot and ringing as it propagates through the space lattice. This effect leads to a numerical noise component which must be filtered before Fourier transformation. Second, Fourier transformation of many lattice-cell field-versus-time waveforms would significantly add to the total requirements for computer storage and execution time [10].

Recent work has shown that very accurate magnitude and phase information for sinusoidal steady-state FD-TD problems can be obtained by method a) above and observing the peak positive- and negative-going excursions of the fields over a *complete cycle* of the incident wave (after having time-stepped through 2-5 cycles of the transient period following the beginning of time-stepping). For certain two- and three-dimensional scattering problems, a dc offset of particular computed field components can be possible. This leads to the following requirements to obtain correct magnitude and phase data:

1) The peak-to-peak value of the sinusoidal response at any point must be observed to eliminate the effects of any dc offset upon the computation of the phasor magnitude.
2) The zero-crossing of the field waveform may not be useful in determining relative phase. Rather, it may be necessary to locate the zero-derivative points of the waveform for this purpose, possibly incorporating an interpolation algorithm to enhance resolution of the relative phase computation without requiring a smaller time step.

As will be shown, this methodology has been found to be successful in achieving ±2.5 percent (or better) and ±3° correspondence of FD-TD results with moment-method computations for two-dimensional canonical problems.

B. Near-Field to Far-Field Transformation

In principle, the solution to electromagnetic scattering by arbitrary conducting bodies leads to the determination of the induced surface electric-current distribution on the body. Then, the induced currents are used to calculate the near or the far fields. However, the surface may have a complex shape or may be loaded with dielectrics in some way as to make a unique problem for each scatterer. A useful alternative would be to obtain the scattered-field information from *off-surface near-field* data, rather than surface-current data. Further, the near-field data could be integrated along arbitrary planar virtual surfaces which completely surround the object of interest. In this manner, accounting of the data would be simple and would be independent of the precise shape of the object which resides within the integration surfaces by using powerful electromagnetic-equivalence relations.

The scattered near field can be transformed conveniently to the far field using an electromagnetic equivalence [18] as shown in Fig. 3. Suppose $(\boldsymbol{E}^s, \boldsymbol{H}^s)$ are the known scattered fields in the region close to the object, which are in fact obtained earlier by the FD-TD analysis. An arbitrary closed virtual boundary surface S_a can be introduced which separates the exterior infinite region B and the interior region A containing the general scatterer. The closed boundary surface S_a is optimally rectangular to conform with distinct planes of the FD-TD lattice located in the scattered-field region (Region 2) of Fig. 2. If $\hat{n}$ is the outward unit normal vector at the surface S_a, then an equivalent problem external to S_a is set up [18] by defining the equivalent tangential electric current $\boldsymbol{J}_{s_{eq}}$ and equivalent tangential magnetic current $\boldsymbol{M}_{s_{eq}}$ on S_a

$$\boldsymbol{J}_{s_{eq}}(r) = \hat{n} \times \boldsymbol{H}^s(r) \tag{4a}$$

$$\boldsymbol{M}_{s_{eq}}(r) = -\hat{n} \times \boldsymbol{E}^s(r). \tag{4b}$$

The equivalent surface currents on S_a produce the same scattered field $(\boldsymbol{E}^s, \boldsymbol{H}^s)$ external to S_a as in the original problem. Region A is now made empty with zero fields and no sources.

The scattered far fields are thus given by the transform of the equivalent currents of (4), over the free-space Green's

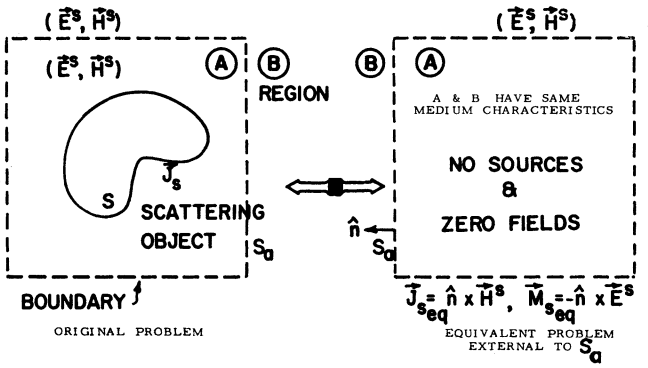

Fig. 3. Electromagnetic equivalence to transform near fields to far fields.

function [22], [23]. If $(\sigma_0, \mu_0, \epsilon_0)$ are the Region-B medium characteristics, we have, with $s = j\omega$, the following scattered-field expressions:

$$H^s(r,s) = -\frac{s}{\gamma_0^2}[\nabla(\nabla \cdot F(r,s)) - \gamma_0^2 F(r,s)] + \frac{1}{\mu_0}\nabla \times A(r,s) \tag{5}$$

$$E^s(r,s) = \frac{s}{\gamma_0^2}[\nabla(\nabla \cdot A(r,s)) - \gamma_0^2 A(r,s)] + \frac{s}{(\sigma_0 + s\epsilon_0)}\nabla \times F(r,s), \qquad r > r_a. \tag{6}$$

In (5) and (6), the electric vector potential is given by

$$F(r,s) = \frac{(\sigma_0 + s\epsilon_0)}{4\pi s}\iint_{S_a} M_{seq}(r_a', s) G(r, r_a'; s)\, dS_a' \tag{7a}$$

$$G(r, r'; s) = \frac{e^{-\gamma_0 |r - r'_a|}}{|r - r_a'|} \tag{7b}$$

$$|r - r_a'| = [(x - x_a')^2 + (y - y_a') + (z - z_a)^2]^{1/2} \tag{7c}$$

and the magnetic vector potential is given by

$$A(r,s) = \frac{\mu_0}{4\pi}\iint_{S_a} J_{seq}(r_a', s) G(r, r_a'; s)\, dS_a' \tag{7d}$$

where the propagation constant is

$$\gamma_0 = [s\mu_0(\sigma_0 + s\epsilon_0)]^{1/2} = jk_0. \tag{7e}$$

Taking the limit $r \to \infty$ gives the required far-field scattering distribution [23].

III. NUMERICAL RESULTS—TWO-DIMENSIONAL CASE

In order to validate the feasibility of this hybrid method to analyze electromagnetic scattering, two canonical two-dimensional conducting and dielectric structures are studied. The numerical results of the FD-TD-computed surface-electric-current distribution, and near electric and magnetic fields are presented for the case of a two-dimensional rectangular metal cylinder subject to a TM-polarized illumination at normal (broadside) incidence. These electric currents and near fields are compared to the MOM-computed results [19], [24]. The scattered-field pattern and the corresponding radar cross section (RCS) are derived from the near- to far-field transformation of the FD-TD data. These are then compared to the results obtained by using the MOM. Additional RCS results for the case of circular metal and dielectric cylinders are also presented. It is shown that a very high degree of correspondence is obtained using this method.

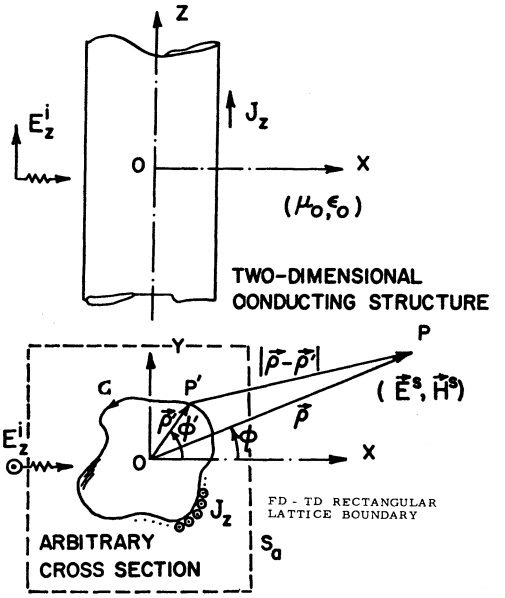

Fig. 4. Geometry of a TM-excited conducting cylinder.

A. Square Cylinder

The scattering by a two-dimensional conducting cylinder of arbitrary cross section is considered first to validate feasibility of the proposed hybrid method. This canonical problem, shown in Fig. 4, is well documented [19], [22], [24]. For the case of a TM-polarized plane-wave excitation, the following integral equation for the surface electric current J_z was solved using MOM:

$$E_z^i(\rho) = \frac{k_0\eta_0}{4}\int_C J_z(\rho') H_0^{(2)}(k_0 |\rho - \rho'|)\, dl', \qquad \rho \in C \tag{8a}$$

$$E_z^i(\rho) = E_0 e^{-jk_0\rho\cos(\phi - \phi^i)}. \tag{8b}$$

In (8a) and (8b), ϕ^i is the angle of incidence (angle between the x axis and the direction of propagation); $H_0^{(2)}$ is the Hankel function of the second kind and zero order; k_0 is the propagation constant in the free-space medium; and η_0 is the intrinsic impedance $= \sqrt{\mu_0/\epsilon_0}$.

The far-field distribution can be obtained from the induced currents J_z as follows:

$$E_z^s(\phi) \sim \frac{k_0\eta_0}{\sqrt{8\pi k_0\rho}} e^{-j(k\rho + \frac{3\pi}{4})}\int_C J_z(x', y') e^{jk_0(x'\cos\phi + y'\sin\phi)} dl' \tag{9a}$$

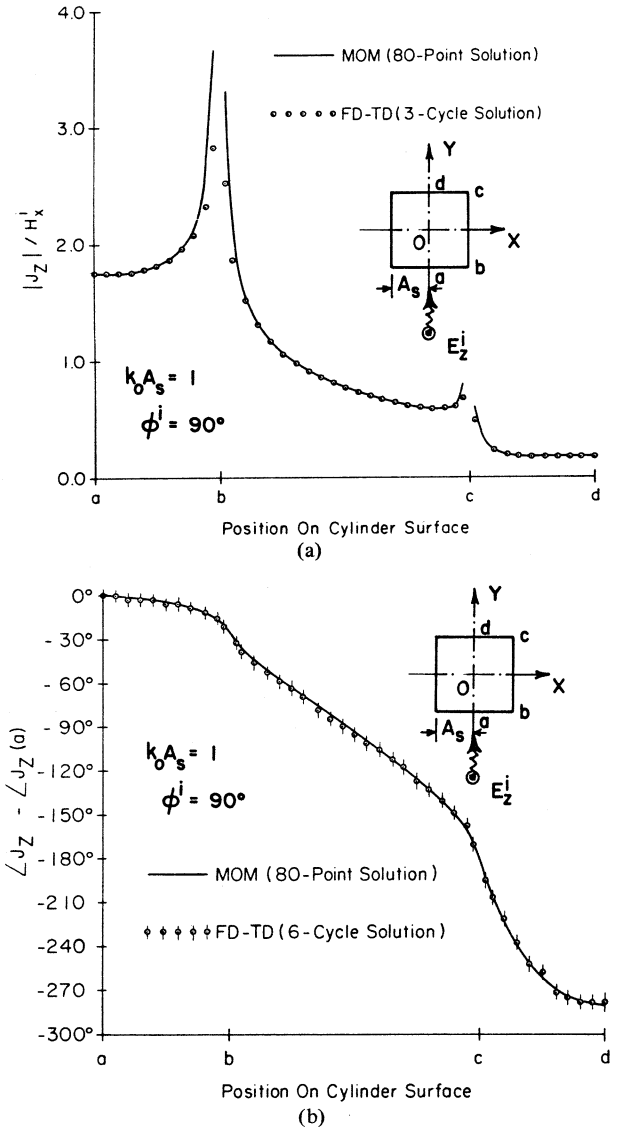

Fig. 5 Comparison of MOM and FD-TD results for magnitude of electric currents on surface of cylinder.

and the scattering radar cross section (RCS) in the far-field region is given by

$$\text{RCS} = 2\pi\rho \left| \frac{E^s(\phi)}{E^i} \right|^2 \quad \lim \rho \to \infty. \tag{9b}$$

We first consider the example of the scattering of a plane wave by a square conducting cylinder. The cylinder has the electrical size $k_0A_s = 1$, where A_s is the half-width of the side of the cylinder. The plane-wave excitation is TM-polarized, with field components $E_z{}^i$ and $H_x{}^i$, and propagates in the $+y$ direction, so that it is at normal incidence to one side of the cylinder ($\phi^i = 90°$). An 84-point MOM solution of (8a) is used as the benchmark for comparison with all FD-TD results, with pulse current expansion and point matching [19], [24].

For the FD-TD analysis, the square cylinder is embedded in a two-dimensional lattice as shown in Fig. 2. Each side of the cylinder spans 20 lattice-cell divisions. The connecting virtual surface between the FD-TD total-field and scattered-field regions is located at a uniform distance of 5 cells from the cylinder surface. Figures 5(a) and (b) graph the comparative results for the FD-TD and MOM analyses of the magnitude and phase of the cylinder surface electric-current distribution for this case. Here, the FD-TD-computed surface current is taken as $\hat{n} \times \boldsymbol{H}_{\tan}$, where $\hat{n}$ is the unit normal vector at the cylinder surface, and $\boldsymbol{H}_{\tan}$ is the FD-TD value of the magnetic field parallel to the cylinder surface, but at a distance of 0.5 space cell from the surface. (The displacement of the $\boldsymbol{H}$ component from the cylinder surface is a consequence of the spatially-interleaved nature of the $\boldsymbol{E}$ and $\boldsymbol{H}$ components of the FD-TD lattice, indicated in Fig. 1.) In Fig. 5(a), the magnitude of the FD-TD-computed surface current agrees with the 80-point MOM solution to better than ±1 percent (±0.09 dB) at all comparison points more than 2 cells from the cylinder edges (current singularities). in Fig. 5(b), the phase of the FD-TD solution agrees with the MOM solution to within ±3° at all comparison points, including the shadow region. The uncertainty bars shown in this figure indicate the present level

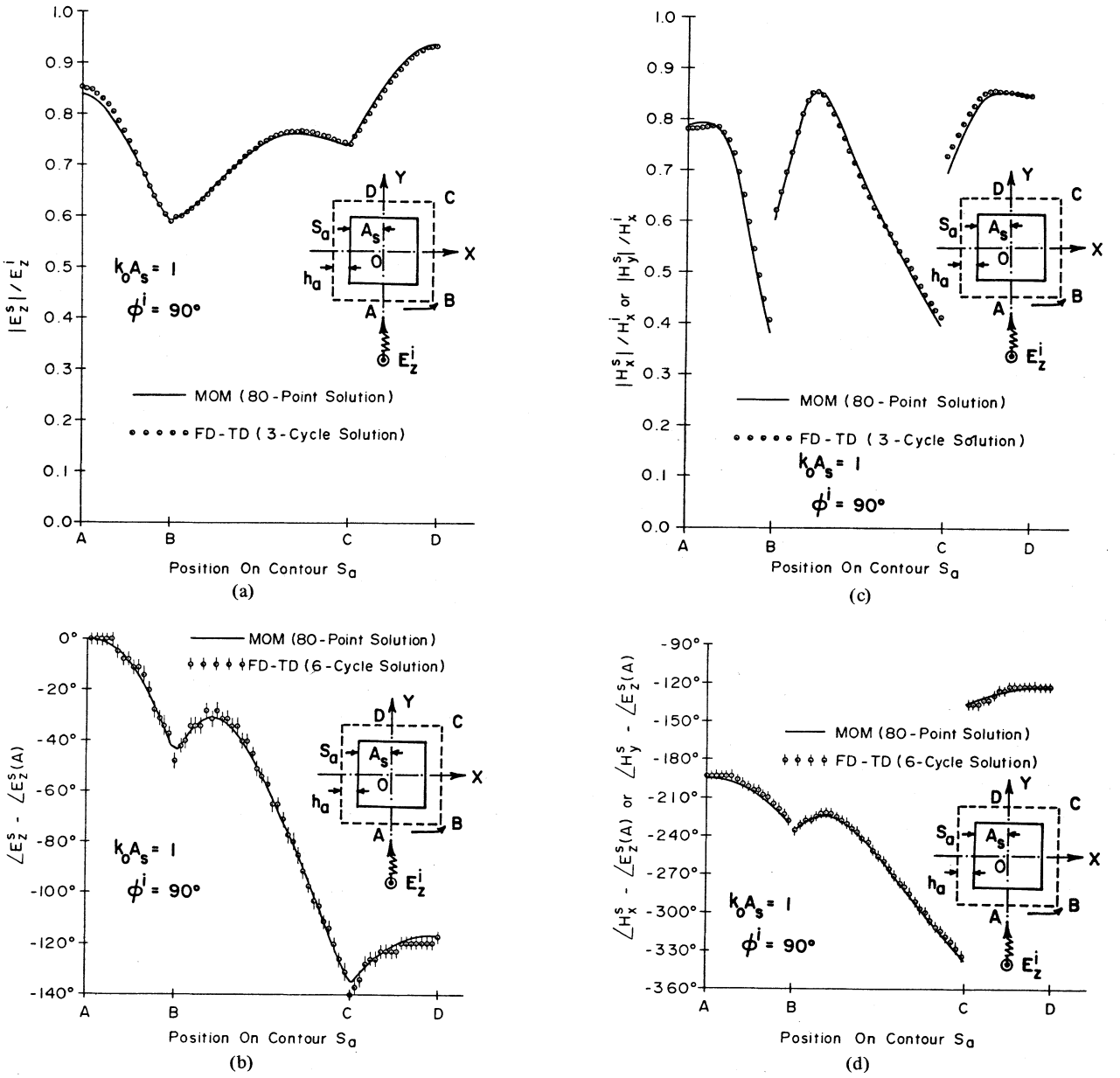

Fig. 6. Comparison of MOM and FD-TD results for phase of near magnetic tangential to contour S_a.

of imprecision in using the FD-TD method to locate the constant-phase points of the computed time-domain $H_{\tan}$ waveform (equivalent to ±1 time step). This imprecision can be reduced in future FD-TD programs by incorporating a simple interpolation algorithm to achieve fractional time-step resolution of points of constant phase.

Fig. 6(a)-(d) shows the comparison of the magnitude and phase of the near-scattered electric and magnetic fields computed by the FD-TD method and MOM. The electric field is tangential to a virtual surface S_a, located at a uniform distance of $h_a = 7$ space cells from the cylinder surface; and the magnetic field is tangential to a virtual surface S_a', located at 6.5 cells from the cylinder surface. Both virtual surfaces are embedded in the scattered-field region of the FD-TD lattice. The level of correspondence between the FD-TD and MOM results is ±2.5 percent (±0.2 dB) and ±3°.

In order to obtain the far-field pattern and the scattering cross section, the near-field to far-field transformation discussed in Section IIB is followed for two-dimensional structures. The near scattered fields shown in Figs. 6(a)-(d) are converted into the corresponding equivalent electric and magnetic current distributions along S_a according to (4a) and (4b). For the two-dimensional case, we have in the far-field region [22], [23]

$$E_z^s = -j\omega\mu_0 \psi_{z_{eq}} + jk_0[-F_{x_{eq}} \sin\phi + F_{y_{eq}} \cos\phi] \quad (10a)$$

where

$$\psi_{z_{eq}} \sim K \int_{S_a} J_{s_{eq_z}}(x', y') e^{+jk_0(x'\cos\phi + y'\sin\phi)}\, dl' \quad (10b)$$

$$F_{x,y_{eq}} \sim K \int_{S_a} M_{s_{eq_{x,y}}}(x', y') e^{+jk_0(x'\cos\phi + y'\sin\phi)}\, dl' \quad (10c)$$

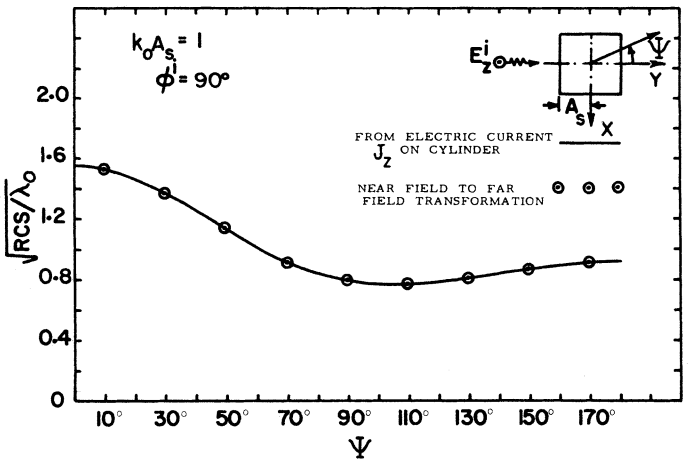

Fig. 7. Scattering cross section of the conducting square cylinder.

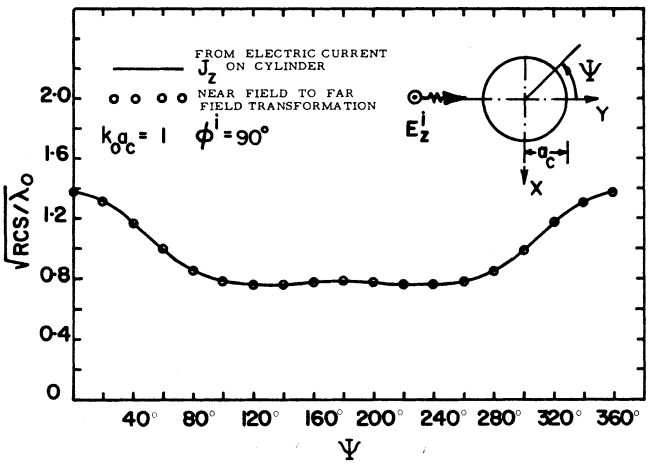

Fig. 9. Scattering cross section of the conducting circular cylinder.

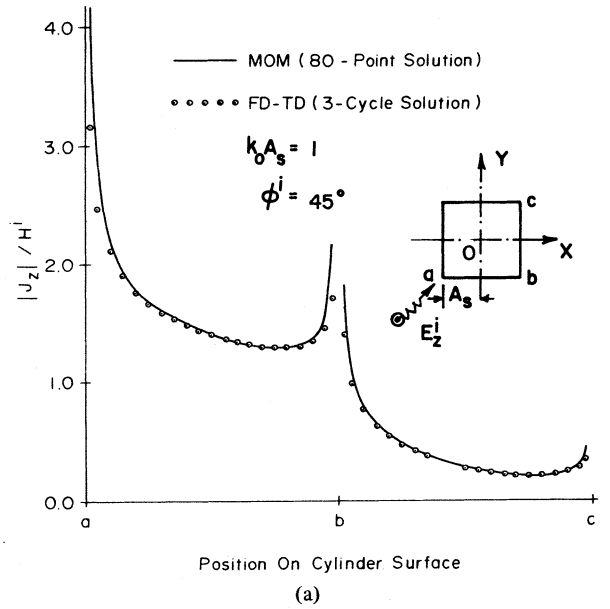

(a)

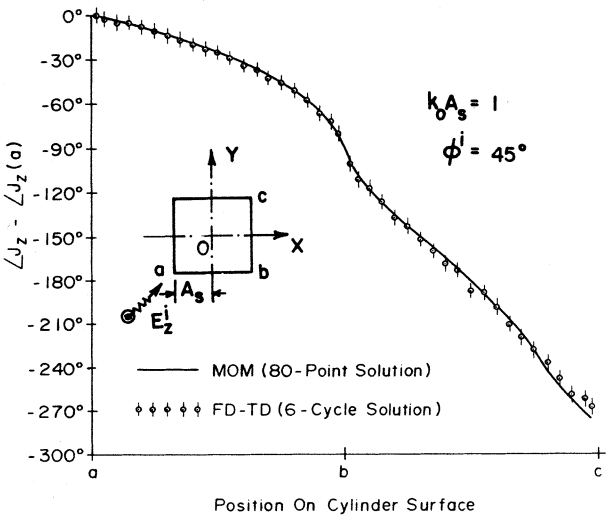

(b)

Fig. 8. Comparison of MOM and FD-TD results for (a) magnitude of electric currents on surface of cylinder oblique-incidence case (ϕ^i = 45°) and (b) phase of electric currents on surface of cylinder oblique-incidence case (ϕ^i = 45°).

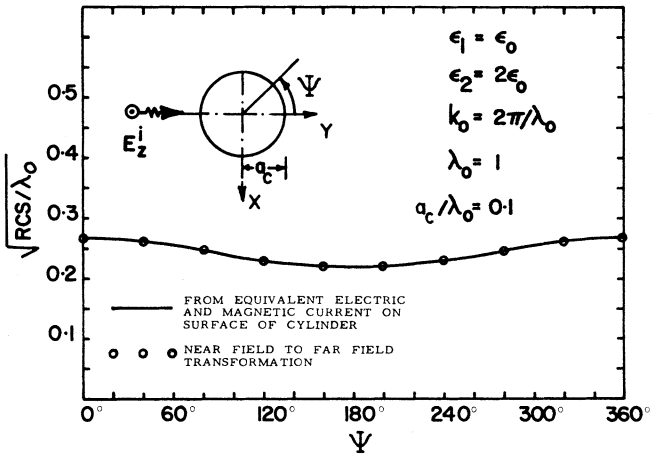

Fig. 10. Scattering cross section of the dielectric circular cylinder.

and

$$K = \frac{e^{-jk_0\rho}}{\sqrt{8\pi k_0 \rho}} e^{-j(3\pi/4)} \tag{10d}$$

and the scattering cross section based on the equivalent currents is given by

$$\mathrm{RCS}_{eq} = 2\pi\rho \left| \frac{E_{eq}^{s}(\phi)}{E^i} \right|^2$$

$$\lim \rho \to \infty . \tag{10e}$$

Fig. 7 shows the scattering cross section of the square conducting cylinder obtained by the near-field (FD-TD data) to far-field transformation. The results agree very well with the scattering cross section derived directly from the electric current on the square cylinder. The validation has also checked for different polarization and incidence angles. For $\phi^i = 45°$ the results of the electric current are shown in Figs. 8(a), (b).

B. Circular Conducting and Dielectric Cylinders

The above analysis using the FD-TD method and the near-field to far-field transformation has also been verified for the

case of a circular conducting cylinder [1] and a circular dielectric cylinder. The results of the scattering cross section are shown in Figs. 9 and 10.

IV. CONCLUSIONS

General electromagnetic-wave scattering problems are difficult to treat. This paper proposes a method to analyze scattering by complex objects by combining the FD-TD method to obtain near scattered fields with a near-field to far-field transformation based on electromagnetic equivalences. To validate the feasibility of this hybrid method, two canonical two-dimensional structures are analyzed and the results are verified with respect to the MOM. This potentially alternative approach has wide application to analyze scattering by structures with complex apertures and dielectric or permeable loadings. Recently, the hybrid method has also been extended to three-dimensional structures, and it has been found to yield the same high accuracy level discussed in this paper for two-dimensional structures.

REFERENCES

[1] J. J. Bowman, T. B. A. Senior, and P. L. E. UsLenghi, Eds., *Electromagnetic and Acoustic Scattering by Simple Shapes*. New York: Wiley, 1969.

[2] K. S. Yee, "Numerical solution of initial boundary value problems involving Maxwell's equations in isotropic media," *IEEE Trans. Antennas Prop.*, vol. AP-14, pp. 302–307, May 1966.

[3] C. D. Taylor, D. H. Lam, and T. H. Shumpert, "Electromagnetic pulse scattering in time-varying inhomogeneous media," *IEEE Trans. Antenna Prop.*, vol. AP-17, pp. 585–589, Sept. 1969.

[4] D. E. Merewether, "Transient currents induced on a metallic body of revolution by an electromagnetic pulse," *IEEE Trans. Electromagn. Compat.*, vol. EMC-13, pp. 41–44, May 1971.

[5] A. Taflove and M. E. Brodwin, "Numerical solution of steady-state electromagnetic scattering problems using the time-dependent Maxwell's equations," *IEEE Trans. Microwave Theory Tech.*, vol. MTT-23, pp. 623–630, Aug. 1975.

[6] A. Taflove and M. E. Brodwin, "Computation of the electromagnetic fields and induced temperatures within a model of the microwave-irradiated human eye," *IEEE Trans. Microwave Theory Tech.*, vol. MTT-23, pp. 888–896, Nov. 1975.

[7] R. Holland, "Threde: A free-field EMP coupling and scattering code," *IEEE Trans. Nucl. Sci.*, vol. NS-24, pp. 2416–2421, Dec. 1977.

[8] K. S. Kunz and K. M. Lee, "A three-dimensional finite-difference solution of the external response of an aircraft to a complex transient EM environment: Part I-The method and its implementation," *IEEE Trans. Electromagn. Compat.*, vol. EMC-20, pp. 328–333, May 1978.

[9] A. Taflove and K. R. Umashankar, "A hybrid moment method/finite difference time domain approach to electromagnetic coupling and aperture penetration into complex geometries," Chap. 14 in *Applications of the Method of Moments to Electromagnetic Fields*, B. J. Strait, Ed. Orlando, FL: SCEEE Press, Feb. 1980.

[10] A. Taflove, "Application of the finite-difference time-domain method to sinusoidal steady-state electromagnetic-penetration problems," *IEEE Trans. Electromagn. Compat.*, vol. EMC-22, pp. 191–202, Aug. 1980.

[11] R. Holland, L. Simpson, and K. S. Kunz, "Finite-difference analysis of EMP coupling to lossy dielectric structures," *IEEE Trans. Electromagn. Compat.*, vol. EMC-22, pp. 203–209, Aug. 1980.

[12] D. E. Merewether, R. Fisher, and F. W. Smith, "On implementing a numeric Huygen's source scheme in a finite-difference program to illuminate scattering bodies," *IEEE Trans. Nucl. Sci.*, vol. NS-27, pp. 1829–1833, Dec. 1980.

[13] R. Holland and L. Simpson, "Finite-difference analysis of EMP coupling to thin struts and wires," *IEEE Trans. Electromagn. Compat.*, vol. EMC-23, pp. 88–97, May 1981.

[14] A. Taflove and K. R. Umashankar, "A hybrid FD-TD approach to electromagnetic wave backscattering," in *1981 URSI/APS-Int. Symp. Proc.* (Los Angeles, CA), June 1981, p. 82.

[15] A. Taflove and K. R. Umashankar, "Solution of complex electromagnetic penetration and scattering problems in unbounded regions," in *Computational Methods for Infinite Domain Media-Structure Interaction*, AMD-Vol. 46, American Society of Mechanical Engineers, Nov. 1981, pp. 83–113.

[16] G. Mur, "Absorbing boundary conditions for the finite-difference approximation of the time-domain electromagnetic-field equations," *IEEE Trans. Electromagn. Compat.*, vol. EMC-23, pp. 377–382, Nov. 1981.

[17] A. Taflove and K. R. Umashankar, "User's code for FD-TD," Final Rep. RADC-TR-82-16 by IIT Research Institute, Chicago, IL to Rome Air Development Center, Griffiss AFB, NY, under Contract F30602-80-C-0302, Feb. 1982.

[18] S. A. Schelkunoff, "Field equivalence theorems," *Comm. Pure Appl. Math.*, vol. 4, pp. 43–59, June 1951.

[19] R. F. Harrington, *Field Computation by Moment Methods*. New York, NY: Macmillan, 1968.

[20] B. Engquist and A. Majda, "Absorbing boundary conditions for the numerical simulation of waves," *Math Comp.*, vol. 31, pp. 629–651, July 1977.

[21] G. A. Kriegsmann and C. S. Morawetz, "Solving the Helmholtz equation for exterior problems with variable index of refraction: I," *SIAM J. Sci. Stat. Comput.*, vol. 1, pp. 371–385, Sept. 1980.

[22] J. Van Bladel, *Electromagnetic Fields*. New York, NY: McGraw-Hill, 1964.

[23] R. F. Harrington, *Time Harmonic Electromagnetic Fields*. New York, NY: McGraw-Hill, 1961, ch. 3.

[24] K. K. Mei and J. Van Bladel, "Scattering by perfectly conducting rectangular cylinders," *IEEE Trans. Antennas Prop.*, vol. AP-11, pp. 185–192, Mar. 1963.